Research Report

Nano-composite Materials for Hydrogen Storage

Yoshitsugu Kojima

Abstract

Chemical hydrides such as MgH_2 are known as high hydrogen containing materials. However their high working temperature and slow kinetics limit their practical application. Mg-based nano-composite materials with nano-Ni catalyst prepared by mechanical milling showed excellent properties, compared with those of Ni, a ball-milled MgH_2 or the mixture of MgH_2 and the nano-Ni catalyst, in terms of the H_2 desorption and absorption. The H_2 absorption capacity at 9 MPa and room temperature in 6 h increased from less than 0.1 wt% for the mixture to 5.0 wt % for the nano-composite material, approaching a maximum of 6.5 wt% in 70 h. The improvement in kinetics is related to the low activation barrier, the large collosion frequency, a short diffusion path length and a high driving force. Carbon-based nano-composite material was synthesized by doping with potassium in superactivated carbon. This material can adsorb 1.6 wt% of hydrogen at room temperature under 5 MPa. This absorption capacity was greater than the value of 1.0 wt% found in potassium-doped graphite. Kinetics of the hydrogen adsorption of the potassium-doped superactivated carbon was considerably improved. The high hydrogen adsorption capacity and the improved kinetics of this system may be derived from the nano-sized graphen and the high surface area.

Keywords Magnesium, Catalyst, Potassium, Activated carbon, Nano-composite material

1. Introduction

A fuel cell is a device that continuously converts the chemical energy of hydrogen (H_2) and oxygen (O_2) into electrical energy. Since the fuel cell has efficiency much higher than that of conventional combustion engines, a fuel cell vehicle (FCV) is expected to have high efficiency.[1)] A polymer electrolyte fuel cell (PEFC, PEM fuel cell) is the prime power source for an FCV. One of the most widely envisioned sources of fuel for the FCV is H_2. Therefore, it is necessary to have a storage tank of H_2 to start the system on demand. The first FCVs were delivered on Dec. 2, 2002. These FCVs feature a 35 MPa H_2 storage tank and can travel 300-355 km on a full tank. The driving ranges of the vehicles are small compared to those of gasoline vehicles. This is the biggest hurdle for FCVs and an improvement in the range is required for a new H_2 storage system.

H_2 can be stored in many different forms, including as compressed or liquefied H_2 in tanks,[1)] by adsorption on activated carbon[1, 2)] and carbon nanotubes,[1, 3)] as a hydrogen-absorbing alloy,[1, 4, 5)] as chemical hydrides such as $NaBH_4$,[6-10)] $NaAlH_4$,[11-14)] MgH_2,[15-18)] $LiBH_4$[19-21)] and metal nitrides,[22-31)] or as organic hydrides (methylcyclohexane, decalin).[32)] Amongst these methods, much attention has been given to thermal decomposition of light weight chemical hydrides (binary hydrides, complex hydrides), consisting of protide H^-, because of their large gravimetric H_2 densities. However, the high working temperature and the slow reaction kinetics (high activation energy) limit the practical application of chemical hydride systems.

In this review, we indicate in the following **Sec. 2**, the fact that the H_2 absorption capacities of the Mg-based nano-composite material with a nano-Ni catalyst exhibited 5.0-6.5 wt% at a high H_2 pressure of 9 MPa and room temperature (296 K). In **Sec. 3**, we demonstrate that kinetics of the H_2 adsorption of carbon-based nano-composite material (potassium-doped superactivated carbon) was considerably improved over conventional K-doped graphite (KC_8+K).

2. Magnesium-based nano-composite materials[33)]

MgH_2 was mechanically milled with nano-Ni 46wt%/Al_2O_3 8wt%/C 46wt% (a nano-Ni catalyst) or a Ni(Soekawa Chemicals, 0.8 μm) catalyst, yielding Mg-based nano-composite materials. The nano-Ni catralyst was prepared by a co-precipitation method. **Figure 1** compares the transmission electron micrographs of the nano-composite materials. The dark portions in Fig. 1(a) and (b) are nano-Ni and Ni whose dimensions are below 100 nm. It is revealed that the products are nano-composite materials.

The Ni crystallite size in the nano-composite materials was calculated using the Scherrer's equation. The Ni crystallite sizes in the nano-composite materials with the nano-Ni and the Ni catalysts were assumed to be 6 nm and 20 nm, respectively. The MgH_2 crystallite size of both the nano-composite materials and the ball-milled MgH_2, as obtained from Scherrer's equation, was 10-11 nm and thus smaller than the value of as-received MgH_2 and the mixture (78 nm). The ball-milled specimens included about 10 % MgO. This contamination might originate from small leaks in the pulverizing system.

Figure 2 shows the desorption curves of the Mg-based nano-composite materials (catalyst: 5 wt%), together with the data from the ball-milled MgH_2 and the mixture. The nano-composite material with the nano-Ni catalyst could desorb 5.8 wt% of H_2 within 6 h at 473 K, followed, in order, by the nano-composite material with the Ni catalyst. The ball-milled MgH_2 and the mixture were unable to desorb

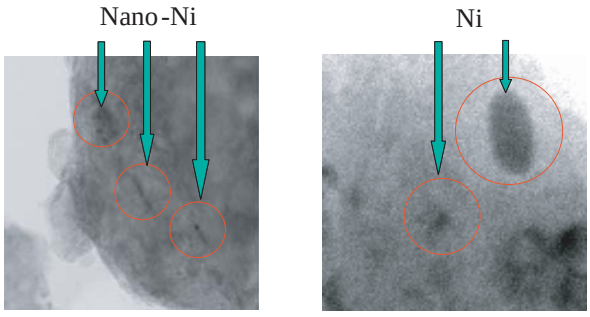

(a) Nano-composite material (nano-Ni/Al_2O_3/C:5wt%)

(b) Nano-composite material (Ni:5wt%)

Fig. 1 TEM photographs of Mg-based nano-composite materials.

H_2 at the temperature. Furthermore, the nano-composite material containing 9 wt% nano-$Ni/Al_2O_3/C$ desorbed 4.9 wt% H_2 at 423 K. We found that H_2 desorption is considerably improved using the nano-Ni catalyst. The maximum H_2 desorption capacities of the nano-composite materials was 6.5 wt% and this was 90 % of the theoretical value (7.2 wt%). This is due to the production of MgO during the mechanical milling.

After H_2 desorption at 523 K, the H_2 absorption curves at room temperature are shown in **Fig. 3**. It can be seen that the H_2 absorption capacities of the nano-composite materials are 4.0-5.0 wt% at 9 MPa and room temperature (296 K), while the H_2 absorption capacity of the ball-milled MgH_2 and the mixture are below 0.1 wt%. The H_2 absorption capacities at 296 K of the nano-composite materials with the Ni catalyst (5 wt%) and the nano-Ni catalyst ($Ni/Al_2O_3/C$: 5-9 wt%) in 70 h were 4.8 wt% and 6.3-6.5 wt%, respectively. At 373 K, the nano-composite materials absorbed 6.3-6.5 wt% of H_2 in 100 sec. The relation between the H_2 absorption capacities of the nano-composite materials and time were given by the first-order rate equation. The initial H_2 absorption rate (rate constant) was independent of the pressure. This result indicates that the concentration of the chemisorbed hydrogen atom in the Ni and the nano-Ni catalysts on the Mg particles linearly increases with pressure. From the Arrhenius plot of k with temperature, the activation energies of the absorption were obtained as 50 and 86 kJ/molH_2 for the nano-composite material with the nano-Ni catalyst and the ball-milled MgH_2, respectively. The activation energy of the nano-composite material is lower than that of the ball-milled pure MgH_2 and corresponds to the value of diffusion in Mg-2 wt% Ce alloy given by Renner and Grabke (40.0 kJ/molH_2).[34] From the Arrhenius plot of H_2 desorption rate constant value with temperature, the activation energy of 74 kJ/molH_2 in the nano-composite material with the nano-Ni catalyst is approximately the same as the standard enthalpy change ($-\Delta H$:74.4-76.2 kJ/molH_2).[35, 36] A possible interpretation of these results is that the activation barrier for dissociation of H_2 molecule and the formation of the hydrogen atom in the nano-composite material is sufficiently low and the absorption rate-limiting step is diffusion-controlled.

The activation energy of desorption for the ball-milled MgH_2 is 144 kJ/molH_2, which is a little smaller than that of unmilled MgH_2 previously reported (156 kJ/molH_2).[37] The activation energy of desorption is, at 162 kJ/molH_2, approximately the sum of the standard enthalpy change (76 kJ/molH_2) and the activation energy of absorption (86 kJ/molH_2).

The height of the activation barrier depends on the

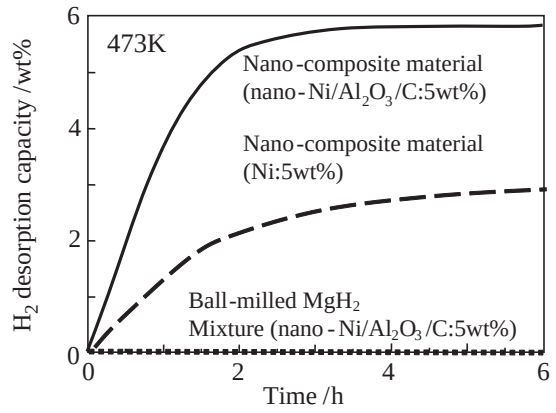

Fig. 2 Hydrogen desorption curves of Mg-based nano-composite materials together with the data from ball-milled MgH_2 and the mixture of MgH_2 and nano-$Ni/Al_2O_3/C$.

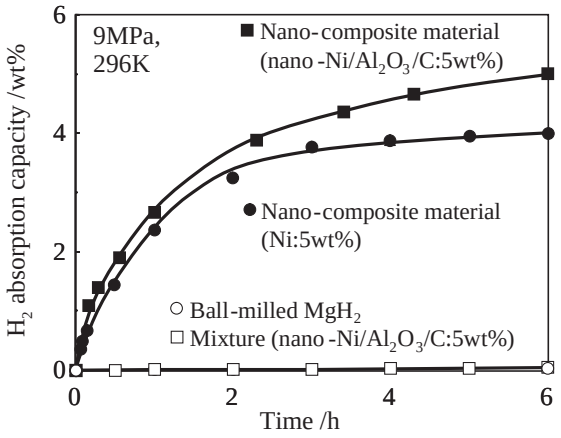

Fig. 3 Hydrogen absorption curves of Mg-based nano-composite materials together with the data from ball-milled MgH_2 and the mixture of MgH_2 and nano-$Ni/Al_2O_3/C$.

surface elements. Without using the catalysts, the activation energy of absorption corresponds to the activation barrier for the dissociation of H_2 molecule and the formation of a hydrogen atom. The activation energies of the H_2 absorption and desorption for the nano-composite material with the Ni catalyst were 52 kJ/molH_2 and 71 kJ/molH_2, respectively. These values are similar to those for the materials with the nano-Ni catalyst, but the rate constant with the nano-Ni catalyst has a higher value. It is suggested that the collision frequency between H_2 molecules and Ni increases with the decreasing size of the Ni catalyst.

It is worth recalling that the milling of the MgH_2, itself, improves the desorption and absorption kinetics over those of the unmilled MgH_2 because of the smaller crystallite size.[37] **Figure 4** shows the concept of a Mg-based nano-composite material and the mixture of MgH_2 and the nano-Ni catalyst. The combination of MgH_2 (Mg) with the smaller crystallites, the nano-Ni catalyst and the high H_2 pressure gives rise to the excellent absorption/desorption kinetics. Recently, in-situ TEM observations of the decomposition and the hydrogenation of the Mg-based nano-composite material has been carried out at 200 kV and 1300 kV TEM.[38] The in-situ TEM observation will be useful in analyzing the mechanism of the H_2 desorption and absorption in nano-composite materials.

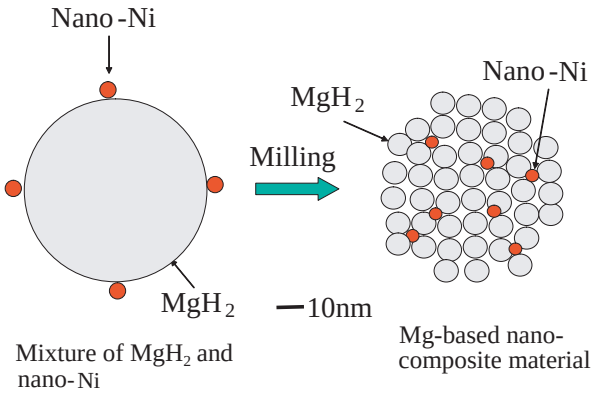

Fig. 4 Conceptual models of Mg-based nano-composite material and the mixture of MgH_2 and nano-Ni.

3. Potassium-doped superactivated carbon[39]

The Raman spectra of superactivated carbon (M-30, Osaka Gas Chemicals Co., Ltd., Japan) and synthetic graphite (MCMB-25-28, Osaka Gas Chemicals Co., Ltd., Japan) are shown in **Fig. 5**. The Raman band observed at 1610 cm^{-1} in single crystallite of graphite is assigned to doubly degenerate deformation vibrations of the hexagonal ring. The additional band at 1340 cm^{-1} is attributed to the size effect in the direction of polycondensed aromatic plane. The crystalline diameter of the carbon in the direction of the polycondensed aromatic plane (diameter of the graphen), La, was obtained by the equation reported by Tuinstra et al.[40] The La of the superactivated carbon was 3.3 nm, and about one seventh of that of synthetic graphite (La: 22 nm). The specific surface areas of the superactivated carbon and the synthetic graphite are 3220 m^2/g and 1 m^2/g, respectively. It should be noted that the maximum specific surface area for carbonaceous materials is well known to be 2630 m^2/g when both sides of graphen are effective for adsorption.[41] The synthetic graphite exhibits sharp XRD peaks, as shown in Fig. 5. The peak at 2θ of 26.4° results from the 002 reflection of the graphite crystallites. Three characteristic peaks of the synthetic graphite, marked by Miller indices (100), (101) and (004), are also observed in the 2θ range from 40° to 60°. The diffraction peaks are not detected in the superactivated

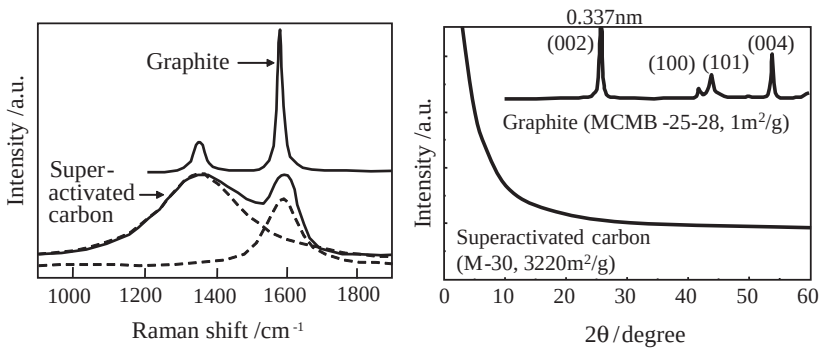

Fig. 5 Raman spectra and X-ray diffraction intensity curves of super-activated carbon and graphite.

carbon. These results suggest that a graphen sheet is dispersed in the carbon. Weighed amounts of superactivated carbon or graphite and K were collected in an inert atmosphere and placed in a self-sealing cell made of stainless steel. The C/K ratio was 4. The cells were then thermally treated at 573 K for 20 h, yielding K-doped carbonaceous materials.

In **Fig. 6**, the amount of H_2 adsorbed in K-doped superactivated carbon at 296 K is shown as a function of time. The H_2 adsorbed attained a value of 1.6 wt% in 10 seconds. When the pressure was reduced to 0.01 MPa, the H_2 desorbed was only 0.1 wt%. Figure 6 also shows the H_2 adsorption capacity of K-doped graphite over time. The capacity gradually increases with time, approaching to a constant value of 1.0 wt%. On decreasing the pressure, H_2 was not desorbed from the graphite. Kinetics of the H_2 adsorption and the H_2 adsorption capacity of the K-doped superactivated carbon were improved with respect to the conventional K-doped graphite. It seems that H_2 adsorption capacity correlates with the structure of the carbon materials. Compared with the graphite, the superactivated carbon used in this work consists small-sized graphen (La: 3.3 nm) and possesses a large specific surface area (3200 m^2/g). These features favor the high adsorption capacity and the improved kinetics of the K-doped superactivated carbon. Compared with 0.4 wt% or zero H_2 adsorption, respectively, measured for the same superactivated carbon and graphite without K-doping as shown in Fig. 2, the high H_2 adsorption may result from the properties of K.

The X-ray diffraction intensity curves of the K-doped carbon materials are shown in **Fig. 7**. Before H_2 adsorption, the K-doped graphite exhibits XRD peaks corresponding to KC_8 and K. The X-ray diffraction peak of hydrogenated K-doped graphite is observed at 2θ of 33° due to $KC_4H_{0.8}$ (003 reflection).[42] **Figure 8** shows the schematic diagram of the layer structure in K-graphite intercalation compounds (KC_8 and $KC_4H_{0.8}$). The intercalation of K and H_2 into KC_8 in the first layer

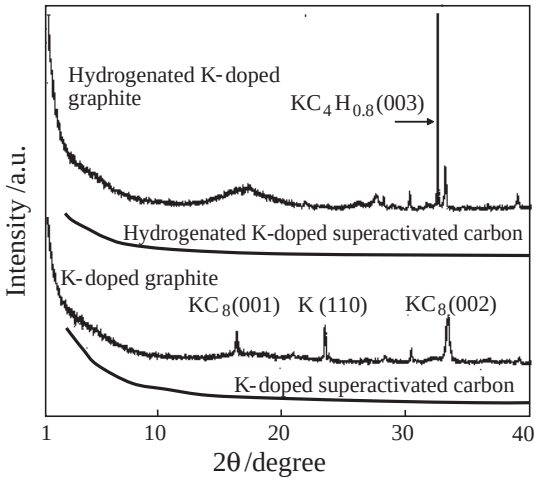

Fig. 7 X-ray diffraction intensity curves of K-doped graphite, hydrogenated K-doped graphite, K-doped superactivated carbon and hydrogenated K-doped superactivated carbon.

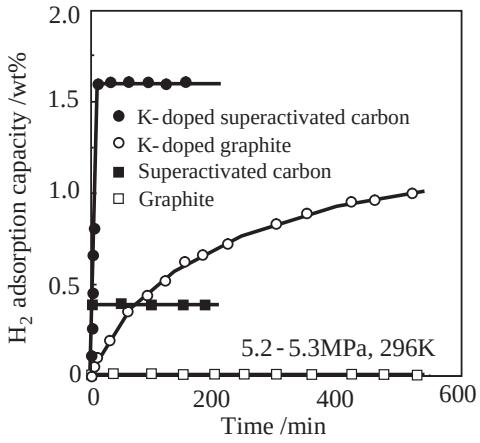

Fig. 6 H_2 adsorbed of K-doped superactivated carbon, K-doped graphite, superactivated carbon and graphite as a function of time.

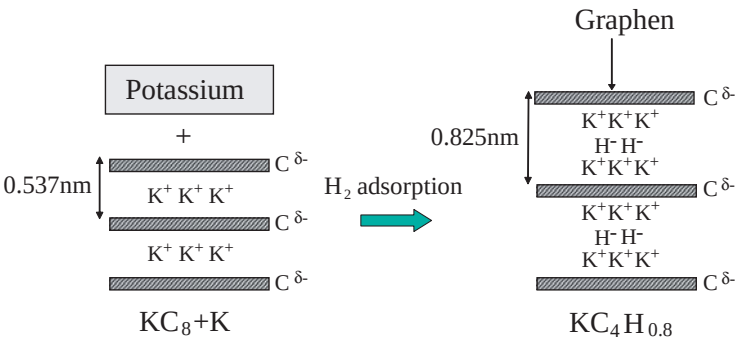

Fig. 8 Schematic diagram of the layer structure in K-graphite intercalation compounds (KC_8 and $KC_4H_{0.8}$).

leads to $KC_4H_{0.8}$in that layer. The compound has a triple atomic layer of K-H-K between graphen planes. X-ray diffraction intensity curves of the K-doped superactivated carbon and the hydrogenated K-doped superactivated carbon were also measured. It is indicated that those specimens possess an amorphous structure, as shown in Fig. 7. The H_2 desorption peak temperatures of the hydrogenated K-doped superactivated carbon (peaks: 567, 649, 773, 1108 K) were different from those of $KC_4H_{0.8}$ (peaks: 532, 697, 884, 1173 K). This can be explained by the fact that the K-doped super-activated carbon includes a new intercalation compound.

4. Conclusions

We investigated H_2 absorption (adsorption) and desorption using nano-composite materials. The Mg-based nano-composite material and K-doped superactivated carbon showed excellent kinetics. The kinetics were improved by producing materials possessing a nano-sized phase.

Acknowledgements

We are greatly indebted to N. Suzuki and Dr. T. Hioki of the Toyota Central R&D Labs., Inc. for their help and discussion.

References

1) Schlapbach, L. and Zuttel, A. : Nature, **414**(2001), 353
2) Chahine, R. and Bose, T. K. : Int. J. Hydrogen Energy, **19**(1994), 161
3) Dillon, A. C., Jones, K. M., Bekkedahl, T. A., Kiang, C. H., Bethune, D. S. and Heben, M. J. : Nature, **386**(1997), 377
4) Tamura, T., Tominaga, Y., Matumoto, K., Fuda, T., Kuriiwa, T., Kamegawa, A., Takamura, H. and Okada, M. : J. Alloys Compd., **330/332**(2002), 522
5) Kojima, Y., Kawai, Y., Towata, S., Matsunaga, T., Shinozawa, T. and Kimbara, M. : Mater. Res. Soc. Symp. Proc., 884E, (2005), GG6.5.1-6.5.8, and J. Alloys Compd., to be published
6) Amendola, S. C., Sharp-Goldman, S. L., Janjua, M. S., Kelly, M. T., Petillo, P. J. and Binder, M. : J. Power Sources, **85**(2000), 186
7) Kojima, Y., Suzuki, K. Fukumoto, K., Sasaki, M., Yamamoto, T., Kawai, Y. and Hayashi, H. : Int. J. Hydrogen Energy, **27**(2002), 1029
8) Kojima, Y., Kawai, Y., Nakanishi, H. and Matsumoto, S. : J. Power Sources, **135**(2004), 36
9) Kojima, Y., Suzuki, K., Fukumoto, K., Kawai, Y., Kimbara, M., Nakanishi, H. and Matsumoto, S. : J. Power Sources, **125**(2004), 22
10) Kojima, Y. and Haga, T. : Int. J. Hydrogen Energy, **28**(2003), 989
11) Bogdanovic, B. and Schwickardi, M. : J. Alloys Compd., **253/254**(1997), 1
12) Bogdanovi, B., Brand, R. A., Marjanovi, A., Schwickardi, M. and Tolle, J. : J. Alloys Compd., **302**(2000), 36
13) Fichtner, M., Engel, J., Fuhr, O., Kircher, O. and Rubner, O. : Mater. Sci. Eng., **B108**(2004), 42
14) Gross, K. J., Thomas, G.. J., Jensen, C. M. : J. Alloys Compd., **330/332**(2002), 683
15) Liang, G., Huot, J., Boily, S., Van Neste, A. and Schulz, R. : J. Alloys Compd., **292**(1999), 247
16) Barkhordarian, G., Klassen, T. and Bormann, R. : J. Alloys Compd., **364**(2004), 242
17) Kojima, Y., Suzuki, K. and Kawai, Y. : J. Mater. Sci. Lett. **39**(2004), 2227
18) Hanada, N., Ichikawa, T. and Fujii, H. : J. Phys. Chem. B, **109**(2005),7188
19) Kojima, Y., Kawai, Y., Kimbara, M., Nakanishi, H. and Matsumoto, S. : Int. J. Hydrogen Energy, **29** (2004), 1213
20) Kojima, Y., Suzuki, K. and Kawai, Y. : J. Power Sources, (2006) in press
21) Zuttel, A., Wenger, P., Rentsch, S., Sudan, P., Mauron, Ph. and Emmenegger, Ch. : J. Power Sources, **118**(2003),1
22) Chen, P., Xiong, Z., Luo, J., Lin, J. and Tan, K. L. : Nature, **420**(2002), 302
23) Kojima, Y. and Kawai, K. : Chem. Commun., (2004), 2210
24) Kojima, Y. and Kawai, Y. : J. Alloys Compd., **395** (2005), 236
25) Luo, W. and Ronnebro, E. : J. Alloys Compd., **404/406**(2005), 392
26) Leng, H. Y., Ichikawa, T., Hino, S., Hanada, N., Isobe, S. and Fujii, H. : J. Phys. Chem. B, **108** (2004), 8763
27) Xiong, Z., Wu, G., Hu, J. and Chen, P. : Adv. Mater., **16**(2004), 1522
28) Orimo, S., Nakamori, Y., Kitahara, G., Miwa, K., Ohba, N., Noritake, T. and Towata, S. : Appl. Phys. A, **79**(2004), 1765
29) Ichikawa, T., Tokoyoda, K., Leng, H. and Fujii, H. : J. Alloys Compd., **400**(2005), 245
30) Nakamori, Y. and Orimo, S. : J. Alloys Compd., **370** (2004), 271
31) Nakamori, Y., Ninomiya, A., Kitahara, G., Aoki, M., Noritake, T., Miwa, K., Kojima, Y. and Orimo, S. : J. Power Sources (2005) in press
32) Newson, E., Haueter, Th., Hottinger, P., Von Roth, F., Scherer, G. W. H. and Schucan, Th. H. : Int. J. Hydrogen Energy, **23**(1998), 905
33) Kojima, Y., Kawai, Y. and Haga, T. : Mater. Res. Soc. Symp. Proc., 837, (2004), N3.5.1-3.5.6
34) Renner, J. and Grabke, H. J. : Metallkd, Z., **6** (1978), 639

35) Yamaguchi, M. and Akiba, E. : Mater. Sci. and Technol., vol. 3B, Ed. by Cahn, R. W., Haasen, P., Kramer, E. J. and Buschow, K. H. J.(1994), 333, VCH (New York)
36) Stampfer, Jr., J. F., Holley, Jr., C. E. and Suttle, J. F. : J. Amer. Chem. Soc., **82**(1960), 3504
37) Huot, J., Liang, G., Boily, S., Van Neste, A. and Schulz, R. : J. Alloys Compd., **293/295**(1999), 495
38) Ohnuki, S., Takase, K., Yashiki, K., Washio, K., Hamada, K., Suda, T. and Kojima, Y. : Collected Abstr. of 2005 Autumn Meet. Jpn. Inst. Met., (2005), 209
39) Kojima, Y. and Suzuki, N. : Appl. Phys. Lett., **84** (2004), 4113
40) Tuinstra, F. and Koenig, J. L. : J. Chem. Phys., **53** (1970), 1126
41) Zuttel, A., Sudan, P., Mauron, P. and Wenger, P. : Appl. Phys. A, **78**(2004), 941
42) Semenenko, K. N., Nalimova., V. A., Klyamkin, S. N. and Bondarenko, G. N. : J. Phys. Chem. Solids, **57** (1996), 915

(Report received on Nov. 21, 2005)

Yoshitsugu Kojima
Research fields : Hydrogen storage materials
Academic degree : Dr. Eng.
Academic Society : Jpn. Inst. Met., Soc. Polym. Sci., Jpn., Soc. Fiber Sci. Technol., Jpn.
Awards : The Awards for Best Posters, Jpn. Soc. High Press. Sci. Technol., 1995
Diploma of Achievement in Sci., Int. Scientists of the Year 2005, Int. Biographical Center, 2005
The Techn. Develop. Award, Jpn. Inst. Met., 2005